BRICHOS domain of Bri2 inhibits islet amyloid polypeptide (IAPP) fibril formation and toxicity in human beta cells

Marie E. Oskarsson[a], Erik Hermansson[b], Ye Wang[a], Nils Welsh[a], Jenny Presto[b], Jan Johansson[b], and Gunilla T. Westermark[a,1]

[a]Department of Medical Cell Biology, Uppsala University, 751 23 Uppsala, Sweden; and [b]Department of Neurobiology, Care Sciences and Society, Division for Neurogeriatrics, Karolinska Institutet, 141 86 Huddinge, Sweden

Edited by F. Ulrich Hartl, Max Planck Institute of Biochemistry, Martinsried, Germany, and approved February 2, 2018 (received for review September 13, 2017)

Aggregation of islet amyloid polypeptide (IAPP) into amyloid fibrils in islets of Langerhans is associated with type 2 diabetes, and formation of toxic IAPP species is believed to contribute to the loss of insulin-producing beta cells. The BRICHOS domain of integral membrane protein 2B (Bri2), a transmembrane protein expressed in several peripheral tissues and in the brain, has recently been shown to prevent fibril formation and toxicity of Aβ42, an amyloid-forming peptide in Alzheimer disease. In this study, we demonstrate expression of Bri2 in human islets and in the human beta-cell line EndoC-βH1. Bri2 colocalizes with IAPP intracellularly and is present in amyloid deposits in patients with type 2 diabetes. The BRICHOS domain of Bri2 effectively inhibits fibril formation in vitro and instead redirects IAPP into formation of amorphous aggregates. Reduction of endogenous Bri2 in EndoC-βH1 cells with siRNA increases sensitivity to metabolic stress leading to cell death while a concomitant overexpression of Bri2 BRICHOS is protective. Also, coexpression of IAPP and Bri2 BRICHOS in lateral ventral neurons of *Drosophila melanogaster* results in an increased cell survival. IAPP is considered to be the most amyloidogenic peptide known, and described findings identify Bri2, or in particular its BRICHOS domain, as an important potential endogenous inhibitor of IAPP aggregation and toxicity, with the potential to be a possible target for the treatment of type 2 diabetes.

islet amyloid | BRICHOS | IAPP | cell death | Bri2

Amyloidoses constitute the largest group of protein-misfolding diseases, in which a given protein aggregates into fibrillar structures rich in β-strand conformations (1). A variety of proteins have been shown to possess the ability to assemble into fibrils with amyloid characteristics, and at least 30 different proteins can form amyloid in humans, each protein associated with a specific disease (2).

Bri2, also known as integral transmembrane protein 2B (ITM2B), is a 266-residue type II transmembrane protein that has been linked to the processing of amyloid precursor protein (AβPP) in Alzheimer disease (AD) (3, 4). Bri2 contains a C-terminal domain, Bri23, released by proteolytic processing between residues 243 and 244 by furin-like proteases (5). Different missense mutations at the stop codon in the *ITM2B* gene cause extended C-terminal peptides ABri or ADan to be released, which by themselves can form amyloid deposits linked to familial British dementia (FBD) (6) and familial Danish dementia (FDD), respectively (7). Bri2 also contains a BRICHOS domain between residues ∼130 and 231 (8), which can be released via processing of ADAM10 (9) and has been shown to bind to the amyloid-β peptide (Aβ) (10), the main component of amyloid plaques in AD. The BRICHOS domain consists of ∼100 residues and is present in over 300 different proteins divided into 12 distinct protein families (11). Protein sequence conservation is low between different BRICHOS proteins, but many share a common overall structure (8, 11, 12). Expression of Aβ fused C-terminally to the BRICHOS domain of Bri2 in transgenic mice results in delayed amyloid formation and intact cognitive performance (13). Bri2 BRICHOS and other BRICHOS domains have been suggested to possess a general antiamyloid chaperone activity, with the ability to bind similar motifs in different proteins (12, 14).

Islet amyloid polypeptide (IAPP) (15) is a beta-cell hormone secreted together with insulin in response to high glucose concentration. IAPP-derived amyloid is present in almost all individuals with type 2 diabetes (T2D), transplanted human islets (reviewed in ref. 16), and, to some extent, also in islets from patients recently diagnosed with type 1 diabetes (17). The initiating events that promote IAPP aggregation are largely unknown, but conditions leading to prolonged beta-cell stress (e.g., high blood glucose and obesity) are associated with islet amyloid formation (18, 19). Oligomeric intermediates produced during the fibril formation process are cytotoxic and believed to be an important cause for the beta-cell loss observed in T2D (20). The paradox that the highly fibrillogenic IAPP remains soluble in islets during nondiabetic conditions, despite being present at high concentrations, may implicate the presence of an endogenous inhibitor of fibril formation in the beta cells.

Significance

Accumulation of islet amyloid polypeptide (IAPP)-containing amyloid fibrils is the main pathological finding in pancreatic islets in type 2 diabetes. The formation of these IAPP amyloid fibrils is considered toxic and may constitute a major cause for the loss of insulin-producing beta cells. The protein domain BRICHOS is present in several different proproteins and possesses antiamyloid chaperone activity. This study demonstrates expression of the BRICHOS-containing protein Bri2 in human pancreatic beta cells and its colocalization with IAPP. The Bri2 BRICHOS domain effectively prevents IAPP from forming fibrils and protects cells from the toxicity associated with IAPP fibrillation. It is concluded that the Bri2 BRICHOS domain may act as an endogenous inhibitor of IAPP amyloid formation in pancreatic beta cells.

Author contributions: M.E.O., E.H., J.P., J.J., and G.T.W. designed research; M.E.O., E.H., Y.W., and G.T.W. performed research; N.W. contributed new reagents/analytic tools; M.E.O., E.H., Y.W., N.W., J.P., J.J., and G.T.W. analyzed data; and M.E.O., E.H., J.P., J.J., and G.T.W. wrote the paper.

The authors declare no conflict of interest.

This article is a PNAS Direct Submission.

[1]To whom correspondence should be addressed. Email: Gunilla.westermark@mcb.uu.se.

This article contains supporting information online at www.pnas.org/lookup/suppl/doi:10.1073/pnas.1715951115/-/DCSupplemental.

Published online March 5, 2018.

In the current study, we aimed to investigate the expression of BRICHOS-containing protein Bri2 in human beta cells and determine its potential role as an inhibitor of IAPP fibril formation and IAPP-induced apoptosis. We show that Bri2 is highly expressed in human pancreatic islets and beta cells and colocalizes with IAPP both intracellularly and in islet amyloid deposits. Moreover, we demonstrate that the Bri2 BRICHOS domain is a potent inhibitor of IAPP fibril formation and IAPP-induced cytotoxicity in vitro and in vivo.

Results and Discussion

Characterization of Bri2 Antibodies. Slot blot analysis against $IAPP_{1–37}$, $Aβ_{1–42}$, and Bri2 proteins corresponding to residues 90 to 236 ($Bri2_{90–236}$) and 113 to 231 ($Bri2_{113–231}$) in human Bri2 protein was performed to characterize the reactivity pattern of two Bri2 antibodies: anti-Bri2 113–231 and anti-Bri2 78–224. None of the Bri2 antibodies cross-reacted with IAPP or Aβ (Fig. 1*A*). Anti-Bri2 113–231 recognized both $Bri2_{90–236}$ and $Bri2_{113–231}$ proteins whereas anti-Bri2 78–224 only recognized $Bri2_{90–236}$ (Fig. 1*A*). The same reactivity pattern was observed when anti-Bri2 113–231 and anti-Bri2 78–224 reactivities to the Bri2 proteins were analyzed with Western blot (Fig. 1*B*). This demonstrates that anti-Bri2 78–224 binding is dependent on residues 90 to 113 of Bri2.

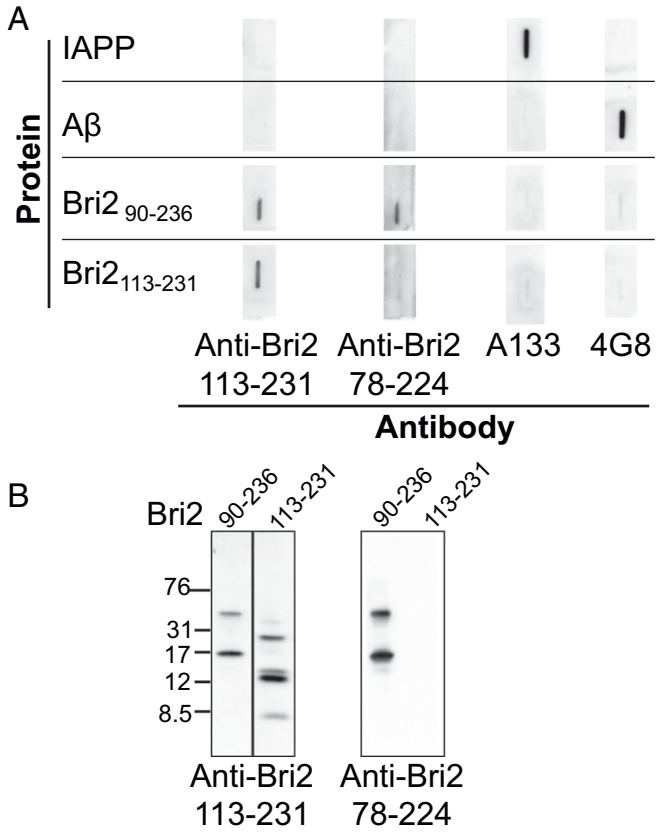

Fig. 1. Mapping reactivity of Bri2 antibodies. (*A*) Reactivities of anti-Bri2 113–231, anti-Bri2 78–224, IAPP antibody A133, and Aβ antibody 4G8 were determined with slot blot analysis against $IAPP_{1–37}$, $Aβ_{1–42}$, $Bri2_{90–236}$, and $Bri2_{113–231}$. No cross-reactivity was observed between Bri2 antibodies and IAPP or Aβ. (*B*) Reactivity of the two Bri2 antibodies with Bri2 proteins was further analyzed with Western blot. Both Bri2 antibodies reacted with the recombinant protein covering residues 90 to 236 of Bri2 (17 kDa) whereas anti-Bri2 78–224 lacked reactivity with the shorter protein corresponding to residues 113 to 231 of Bri2 (14 kDa). Migration of marker proteins with given molecular masses in kDa are indicated.

Bri2 Reactivity in Human Islets and the Human Beta-Cell Line EndoC-βH1. Distribution of the Bri2 protein in extra neuronal tissues is not well-studied, and therefore we first examined whether Bri2 was present in the islets of Langerhans and, if so, in which cells. Bri2 reactivity was detected in extracts from human islets with both Bri2 antibodies (Fig. 2). Bri2 113–231 antiserum detected proteins with molecular masses of ∼15 kDa, 30 kDa, and 35 kDa (Fig. 2*A*) whereas the Bri2 78–224 antibody mainly detected a 35-kDa protein. However, when increasing the exposure time, weak reactivity with proteins of lower molecular masses was observed (Fig. 2*B*). The predicted molecular mass for Bri2 is 30 kDa, but it has been observed to migrate as a slightly larger protein in SDS/PAGE, and N-glycosylation of Asp170 has been reported, which would add ∼2 kDa (21). Full-length Bri2 (266 residues, ∼30 kDa) can be proteolytically processed by furin and ADAM10 releasing the C-terminal Bri23 peptide (23 residues, ∼3 kDa) and the BRICHOS domain (107 residues, ∼13 kDa), leaving a membrane-bound fragment (136 residues, ∼15 kDa) (Fig. 2*C*). These predicted molecular masses of processed Bri2 fragments agree well with the protein pattern observed with Western blot analysis of islet extracts, given that the proteins migrate at slightly higher molecular masses. The 15-kDa protein, possibly the released BRICHOS domain (predicted molecular mass of 13 kDa), was only recognized by anti-Bri2 113–231 (Fig. 2*A*) since N-terminal processing of the BRICHOS domain precludes recognition by anti-Bri2 78–224 shown to be dependent on residues 90 to 113 (Fig. 1*B*).

Islets contain five different endocrine cell types, of which the most prevalent are insulin-producing beta cells and glucagon-producing alpha cells. Bri2 antibodies demonstrated a similar reactivity pattern in EndoC-βH1 cells (pure beta cells) compared with human islets, demonstrating that at least part of the reactivity in islets is derived from the beta cells (Fig. 2 *A* and *B*). The presence of Bri2 in islet beta cells was confirmed by double immunolabeling of human pancreas sections where Bri2 was detected in insulin-positive cells (Fig. 2 *D–F*). Bri2 reactivity was also detected in glucagon-positive alpha cells and somatostatin-positive delta cells (Fig. S1), with no or very little Bri2 in surrounding exocrine pancreas tissue. Bri2 mRNA was detected in human islets, and levels remained unaltered during exposure of islets to high glucose for 2 d, a condition that increased IAPP mRNA levels ∼40-fold (Fig. S2). Double immunolabeling revealed the presence of Bri2 in insulin-positive EndoC-βH1 cells (Fig. 2 *G–I*), and Bri2 reactivity appeared in subcellular compartments partly colocalizing with the trans-Golgi marker TGN38 (Fig. 2 *J–L*). No colocalization between Bri2 immunoreactivity and ER or lysosomal markers was observed (Fig. S3). Although the Bri2 protein must be present in ER during synthesis, it appears to accumulate in, or in compartments close to, the trans-Golgi apparatus, reaching the threshold level of detection with the immunodetection method used. Weak Bri2 reactivity is also identified in beta-cell compartments corresponding to areas positive for insulin: i.e., secretory granules (Fig. 2*G*).

IAPP and Bri2 Colocalize in Islet Amyloid Deposits in Patients with T2D. Bri2 has mostly been studied in the context of neurodegenerative diseases such as AD where inhibiting effects of the Bri2 BRICHOS domain on Aβ amyloid formation (10, 22–25) and on AβPP processing (3, 4) have been described. Our finding of Bri2 expression in beta cells, the same cells that express the highly fibrillogenic IAPP peptide, warranted analysis of whether any colocalization between Bri2 and the amyloid peptide exists. For this purpose, we chose the highly specific and sensitive antibody-based detection method in situ proximity ligation assay (PLA), which generates signals if antibody targets colocalize within 40 nm from each other. A combination of both Bri2 antibodies was used as positive control, which expectedly generated intense red fluorescent intracellular PLA signals in EndoC-βH1 cells (Fig. 3*A*).

CELL BIOLOGY

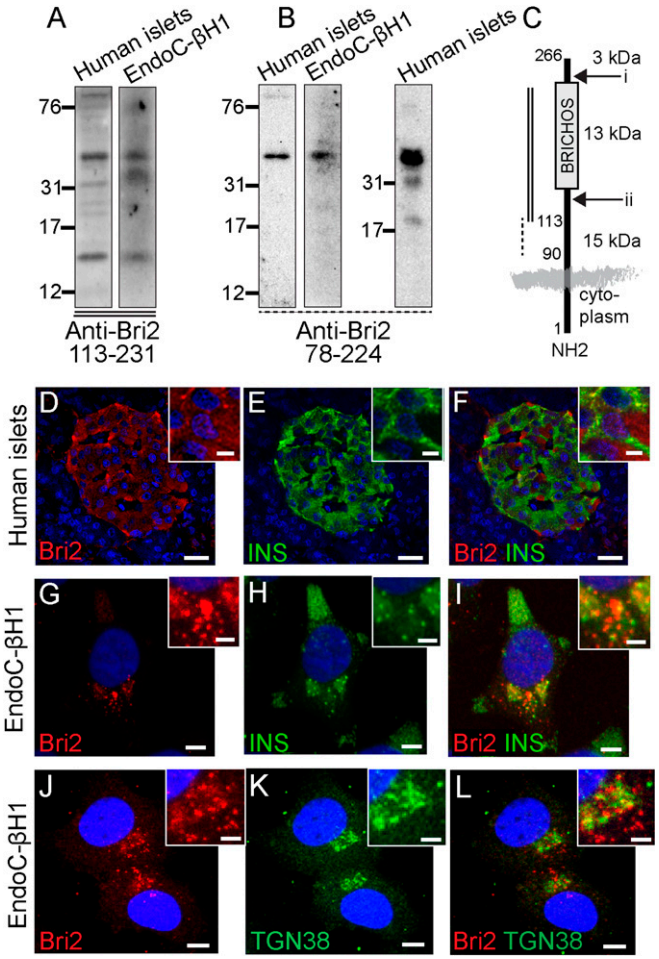

Fig. 2. Bri2 reactivity in human islets and the human beta-cell line EndoC-βH1. Extracts of isolated human islets and human EndoC-βH1 cells were analyzed with Western blot using anti-Bri2 113–231 (*A*) and anti-Bri2 78–224 (*B*). Anti-Bri2 113–231 detected proteins with molecular mass of 15 kDa, 30 kDa, and 35 kDa in both human islets and EndoC-βH1 cells. Anti-Bri2 78–224 mainly detected the 35-kDa protein, but, when increasing the exposure time, weak reactivity with proteins of lower molecular masses was observed. Migration of marker proteins with given molecular masses in kDa are indicated. (*C*) Schematic overview of Bri2 and its processing by (i) furin and (ii) ADAM10 with predicted molecular masses of generated fragments. Box shows the BRICHOS domain. Bri2 antibody epitopes are indicated to the left with the same symbols as in *A* and *B*. (*D–F*) Human pancreas section double-immunolabeled with anti-Bri2 113–231 and insulin antibodies revealed Bri2 reactivity in cells positive for insulin. (*G–I*) Bri2 reactivity was also detected in the insulin-positive EndoC-βH1 cells using anti-Bri2 78–224, which (*J–L*) appeared in subcellular compartments partly colocalizing with trans-Golgi marker TGN38. Nuclei stained with DAPI (blue). Images are merged z-stacks acquired with confocal microscopy. (Scale bars: *D–F*, 20 μm, *Insets*, 10 μm; *G–L*, 5 μm, *Insets*, 2 μm.) INS, insulin.

The combination of anti-Bri2 113–231 with IAPP antibody A133 also generated intracellular PLA signals (Fig. 3*B*), as did the combination of anti-Bri2 78–224 with IAPP antibody SM1341 (Fig. S4). The intracellular colocalization of Bri2 and IAPP was anticipated since both occur in the ER and Golgi apparatus.

The next question was whether Bri2 and IAPP colocalized in extracellular islet amyloid deposits. To analyze this, pancreas sections from a patient with type 2 diabetes containing islet amyloid (Fig. 3*C*) were incubated with anti-Bri2 113–231 combined with IAPP antibody A133, and numerous PLA signals were generated throughout areas corresponding to islet amyloid (Fig. 3*D*). PLA signals originated from amyloid deposits and not from intracellular colocalization of IAPP and Bri2 since an islet free from amyloid did not generate any PLA signals (Fig. S5). It is possible that the harsher fixation treatment of human postmortem material abolished recognition of the intracellular colocalization of IAPP and Bri2 observed in the more mildly fixed EndoC-βH1 cells. Combining anti-Bri2 78–224 with IAPP antibody SM1341 did not result in any PLA signals in islet amyloid (Fig. S5). As anti-Bri2 78–224 did not detect the Bri2 BRICHOS domain (Figs. 1*B* and 2*B*), it is possible that a Bri2 fragment processed N-terminally of the BRICHOS domain rather than unprocessed Bri2 is associated with islet amyloid deposits. Immunohistochemical studies have shown that Aβ and Bri2 colocalize in amyloid plaques in AD brains (26), and, as a positive control for the in situ PLA, anti-Bri2 113–231 was combined with Aβ antibody 4G8, which generated PLA signals in Congo red-positive plaques in brain sections from a patient with AD (Fig. 3 *E* and *F*).

Bri2 BRICHOS Prevents in Vitro Amyloid Fibril Formation of IAPP. The observed colocalization of Bri2 and IAPP in beta cells and islet amyloid suggests a role for Bri2 in the kinetics of IAPP fibril

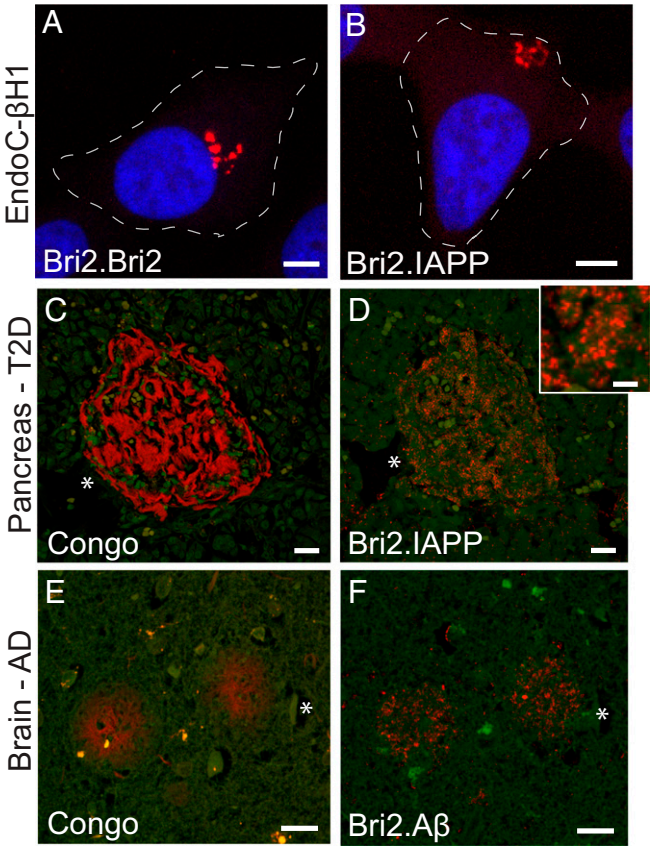

Fig. 3. IAPP and Bri2 colocalize in human beta cells and islet amyloid. Proximity ligation assay (PLA) was performed in (*A*) EndoC-βH1 cells with anti-Bri2 113–231 combined with anti-Bri2 78–224 as positive control and, as expected, generated intracellular PLA signals seen as red fluorescent spots. Anti-Bri2 113–231 combined with IAPP antibody A133 generated PLA signals intracellularly in (*B*) EndoC-βH1 cells and (*D*) in extracellular islet amyloid deposits in a pancreas section from a patient with T2D. (*C*) Congo red was used to identify amyloid in an adjacent section. (*E* and *F*) Anti-Bri2 113–231 combined with Aβ antibody 4G8 generated PLA signals in Congo red-positive amyloid plaques in cortical brain sections from a patient with Alzheimer disease. Asterisks denote corresponding regions in image pairs. Images are merged z-stacks acquired with confocal microscopy. (Scale bars: *A* and *B*, 5 μm; *C–F*, 20 μm; *Inset*, 2 μm.) Nuclei stained with DAPI (blue). The cell borders are indicated with dashed white lines in *A* and *B*.

formation. In vitro fibril formation was monitored with a Thioflavin T (ThT) binding assay in Krebs-Ringer glucose Hepes (KRGH) buffer, pH, 7.4 at 37 °C using freshly dissolved IAPP alone or in the presence of recombinant Bri2 protein covering residues 113 to 231 comprising the BRICHOS domain (Bri2 BRICHOS). IAPP was diluted from a stock solution to a final concentration of 50 μM immediately before the assay. After an ∼1.5-h-long lag phase, fibril formation was seen by a sudden increase in ThT fluorescence (Fig. 4*A*). Presence of 5 μM Bri2 BRICHOS from the start of the assay completely prevented any increase in ThT signal, and the inhibiting effect lasted for an extended time period (>150 h). Control experiments verified that Bri2 BRICHOS did not interfere with the binding between ThT and amyloid fibrils (Fig. S6), and another amyloid-specific dye, Congo red, detected only few deposits in IAPP+Bri2 BRICHOS samples analyzed after >57 h incubation (Fig. S7). In addition, transmission electron microscopy (TEM) analyses of negatively stained IAPP+Bri2 BRICHOS 4-h samples confirmed the absence of any fibrillar material. Instead, amorphous, irregular-shaped aggregates with IAPP and Bri2 immunoreactivity were observed (Fig. 4 *C*–*E*). No such aggregates were observed when Bri2 BRICHOS was incubated alone. In contrast, IAPP incubated without Bri2 BRICHOS for 4 h was assembled into long, ∼10-nm-wide fibrils (Fig. 4*B*). The inhibiting effect of Bri2 BRICHOS on amyloid fibril formation was observed also in the presence of cells that expose cell surface components known to promote fibril formation, such as phospholipids (27) and heparan sulfate proteoglycans (28) (Fig. 4*F*).

Addition of Bri2 BRICHOS at a 1:1 ratio to IAPP from the start or during the lag phase revealed complete inhibition of fibril formation (Fig. 5*A*). Addition during the elongation phase resulted in an abrupt flattening of the ThT curve. At higher IAPP concentrations (10:1 ratio) only addition of Bri2 BRICHOS from the start could completely prevent fibril formation during the analyzed time period. Addition during lag phase at a 10:1 ratio resulted in delayed fibril formation from ∼1 h to >15 h, and addition during elongation phase had no inhibiting effect (Fig. 5*B*).

Bri2 BRICHOS prevents Aβ from forming fibrils by keeping it in a monomeric form during an extended lag phase (22). Although our TEM analyses revealed large amorphous aggregates in IAPP+Bri2 BRICHOS samples, we explored the possibility that some IAPP molecules were kept as monomers using size-exclusion chromatography (SEC) combined with immunoblotting of eluted fractions. A column with the exclusion limit of 2,000 kDa was used to exclude entry of any fibrils or aggregates

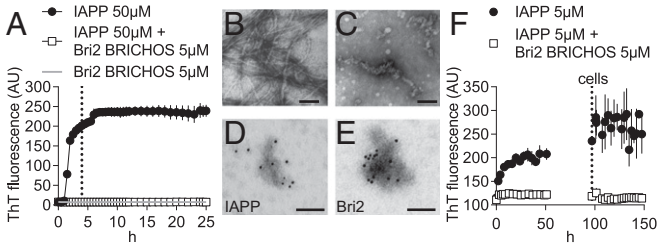

Fig. 4. Bri2 BRICHOS prevents IAPP fibril formation. Fibril formation of 50 μM IAPP alone or in the presence of 5 μM recombinant Bri2 BRICHOS was monitored with 3 μM Thioflavin T (ThT) in KRGH buffer, pH 7.4, at 37 °C at 480 nm emission with 440 nm excitation. (*A*) IAPP alone formed fibrils after ∼1.5-h-long lag phase whereas fibril formation was completely abolished in the presence of Bri2 BRICHOS. Transmission electron microscopy analysis of negatively stained samples recovered at 4 h revealed (*B*) typical amyloid fibrils from IAPP samples whereas (*C*) IAPP+Bri2 BRICHOS samples contained large amorphous aggregates positive for (*D*) IAPP and (*E*) Bri2 antibodies. Immuno-EM performed with IAPP antibody A133 or anti-Bri2 113–231 and reactivity detected with 10-nm gold particles. (Scale bars: 100 nm.) (*F*) Addition of CHO cells (∼20,000 per well) did not affect ThT signals from IAPP+Bri2 BRICHOS samples. Each data point represents mean ± SD (n = 3 to 4).

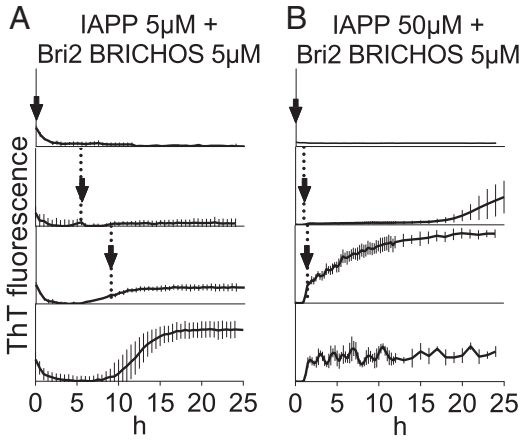

Fig. 5. Bri2 BRICHOS added at different time points during IAPP fibril formation. Addition of 5 μM Bri2 BRICHOS (arrows) at different time points during fibrillation of (*A*) 5 μM IAPP or (*B*) 50 μM IAPP revealed inhibition of fibril formation when Bri2 BRICHOS was added from the start or during lag phase. Addition during the elongation phase resulted in a flattening of the ThT curve in 5 μM IAPP but had no effect when added during the elongation phase of 50 μM IAPP. Fibril formation of IAPP 5 μM and 50 μM without any additions is shown in the bottom graphs. Same scale on the y axis within *A* and within *B*. Each data point represents mean ± SD (n = 4).

containing more than ∼500 IAPP monomer subunits. Freshly dissolved IAPP applied to the column eluted as dimers and trimers between 16 and 19 mL and monomers at 22 mL (Fig. 6*A*). However, neither IAPP alone nor IAPP+Bri2 BRICHOS incubated for 4 h at 37 °C contained any detectable monomers, suggesting that all IAPP monomers had assembled into larger aggregates, or fibrils for IAPP alone, unable to enter the column. Bri2-positive fractions eluting between 5 and 10 mL were detected in IAPP+Bri2 BRICHOS samples, which were not seen with Bri2 BRICHOS alone (Fig. 6*B*). These fractions also displayed some IAPP reactivity, suggesting that they contained aggregates of IAPP and Bri2 BRICHOS small enough to enter the column. Taken together, our results demonstrate that Bri2 BRICHOS prevents IAPP from forming amyloid fibrils and that IAPP is instead redirected to an off-pathway, in which amorphous aggregates with incorporated or bound Bri2 BRICHOS are formed.

Bri2 BRICHOS Binds to IAPP Fibrils and Reduces Seeding Capacity. The formation of amyloid fibrils has been proposed to occur via at least three pathways: aggregation of monomers into small nuclei by primary nucleation, incorporation of monomers onto existing fibril ends, and formation of new fibrils by a catalytic reaction on the surface of existing fibrils, called secondary nucleation (29). Recently, proSP-C BRICHOS was demonstrated to inhibit Aβ42 aggregation by binding to the surface of Aβ42 fibrils and prevent secondary nucleation (30). The observed colocalization of Bri2 with IAPP in islet amyloid deposits (Fig. 3*D*) suggests that Bri2 BRICHOS could have a similar mode of action on IAPP fibrillation. To test this, we incubated preformed IAPP fibrils formed from 50 μM IAPP with 5 μM Bri2 BRICHOS for 3 h at 37 °C, followed by TEM analysis of the fibrils using anti-Bri2 113–231 and negative stain. Results show that all Bri2 immunoreactivity colocalized with the IAPP fibrils (Fig. 7 *A* and *B*). Also, we determined if Bri2 BRICHOS affected the seeding capacity of IAPP fibrils. Preformed fibrils of 5 μM IAPP were incubated with 1, 5, 10, and 20 μM Bri2 BRICHOS for 3 h and washed twice in KRGH. Decorated or undecorated preformed fibrils (final concentration equivalent to 500 nM monomeric IAPP) were added as seed to IAPP (5 μM), and aggregation was monitored with a ThT assay. The presence of undecorated fibrils

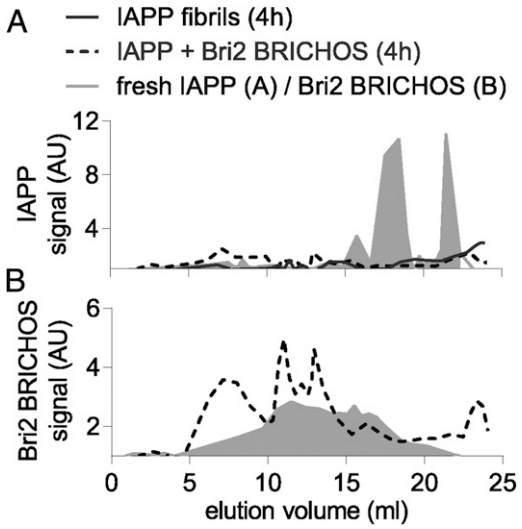

Fig. 6. Bri2 BRICHOS does not keep IAPP as monomers. Samples of 50 μM IAPP or 50 μM IAPP with 5 μM Bri2 BRICHOS incubated for 4 h at 37 °C or freshly diluted IAPP (50 μM) or Bri2 BRICHOS (5 μM) were separated on a Superose-12 column, and eluted fractions were analyzed for (*A*) IAPP reactivity and (*B*) Bri2 reactivity. Fresh IAPP eluted as monomers, dimers, and trimers between 16 and 22 mL whereas neither IAPP incubated alone or in the presence of Bri2 BRICHOS for 4 h contained any monomers, in accordance with the formation of fibrils and large amorphous aggregates seen in Fig. 4 *B* and *C*. Bri2 reactivity revealed a left-shift in the elution profile of Bri2 BRICHOS after incubation with IAPP for 4 h, indicating presence of larger molecular weight species. These species eluting between 5 and 10 mL also contained some IAPP reactivity. AU, arbitrary units.

resulted in a dramatic reduction of the lag phase, compared with samples without seeds (Fig. 7*C*). However, IAPP fibrils incubated with Bri2 BRICHOS displayed a reduced seeding capacity as evidenced by a right-shifted ThT curve, compared with uncoated IAPP fibrils. The degree of inhibition depended on the Bri2 BRICHOS concentration used, and fibrils incubated with 1 μM Bri2 BRICHOS delayed fibrillation 2 h compared with undecorated fibrils (Fig. 7*C*). IAPP fibrils incubated with 5 and 10 μM Bri2 BRICHOS displayed a marked reduction of the seeding capacity, approaching the 6-h lag phase of unseeded IAPP. This proposes interference with secondary nucleation as one mechanism for Bri2 BRICHOS inhibition of IAPP fibril formation. The seeding capacity was abolished for seeds incubated with 20 μM Bri2 BRICHOS. These decorated fibrils also delayed fibrillation of 5 μM IAPP. This result could be due to a disassociation of Bri2 BRICHOS from the decorated fibrils. Presence of Bri2 BRICHOS at the start of IAPP aggregation prevented fibrillation of IAPP as shown in Fig. 5. The amorphous aggregates of IAPP+Bri2 BRICHOS described in Fig. 4*C* exhibited no seeding activity, consistent with their lack of fibrillar structure (Fig. S8).

Ratio-Dependent Rescue Effect of Bri2 BRICHOS on IAPP-Induced Apoptosis. While Bri2 BRICHOS-inhibiting effects on in vitro IAPP fibril kinetics are intriguing, the biologically relevant question is whether it also limits IAPP-induced toxicity. It is likely that IAPP exerts cellular toxicity via both intracellular (31, 32) and extracellular fibril formation (33). The effect of Bri2 BRICHOS on apoptosis induced by extracellular IAPP fibrillation was investigated using CHO cells expressing a FRET-based reporter for caspase-3 activation (28). The reporter consists of two fluorophores connected via a short Asp-Glu-Val-Asp (DEVD)–containing linker, and cleavage of the linker by active caspase-3 during apoptosis results in loss of FRET between the fluorophores. All IAPP solutions were diluted from a stock solution immediately before addition to the cells. Incubation of CHO-DEVD cells with increasing concentrations of IAPP mixed with sonicated preformed IAPP fibrils (seed) resulted in a concentration-dependent loss of FRET: i.e., caspase-3 activation over time (Fig. 8*A*). Exposure of cells to the different concentrations of IAPP (5, 10, 20, 40, and 50 μM) mixed with Bri2 BRICHOS at a constant concentration of 5 μM from start revealed an inhibiting effect of Bri2 BRICHOS on IAPP-induced toxicity at 5 μM and 10 μM IAPP (Fig. 8). However, when the ratio exceeded 4:1 (20 μM IAPP:5 μM Bri2 BRICHOS), the rescue effect was lost (Fig. 8) although fibril formation was restrained according to results from the ThT assay (Fig. 4*A*).

Bri2 BRICHOS Domain Protects EndoC-βH1 from Cell Death Induced by High Glucose and High Sodium Palmitate Concentrations. To investigate the role of Bri2 under conditions of beta-cell stress when the risk of IAPP aggregation is high, we used siRNA

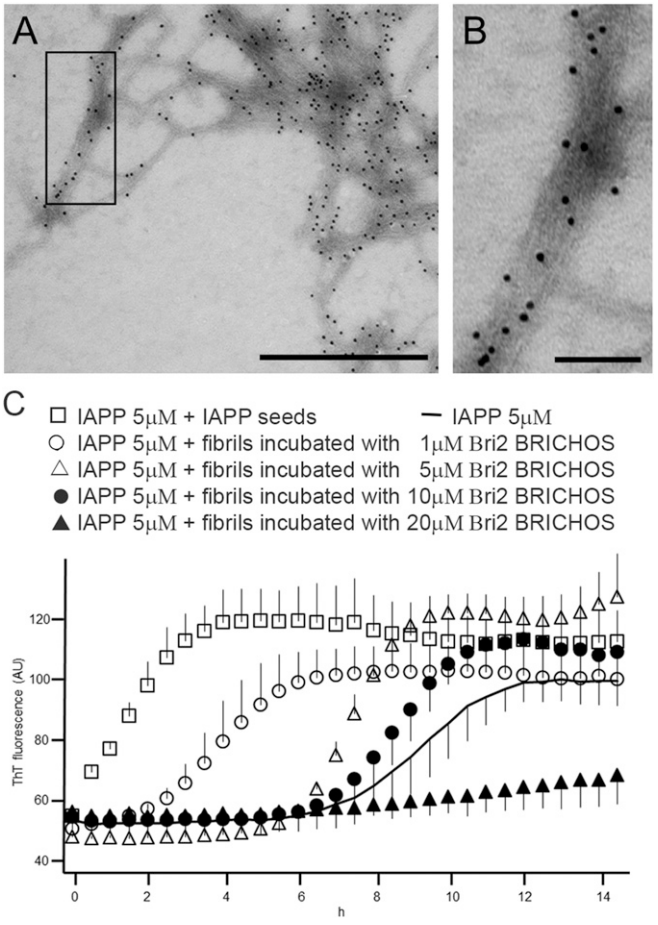

Fig. 7. Bri2 BRICHOS binds to IAPP fibrils and reduces seeding potency. (*A*) Preformed IAPP fibrils were incubated with 5 μM Bri2 BRICHOS for 3 h at 37 °C. Transmission electron microscopy revealed Bri2 immunoreactivity detected with secondary antibodies conjugated with 10-nm gold particles decorating the bundles of fibrils. (*B*) Magnification of boxed area in *A*. (Scale bars: *A*, 500 nm; *B*, 100 nm.) (*C*) Preformed fibrils decorated with 1, 5, 10, and 20 μM Bri2 BRICHOS were diluted and added as seeds (final concentration corresponding to 500 nM monomeric IAPP) to 5 μM IAPP, and fibril formation was monitored with ThT assay. Bri2 BRICHOS-coated fibrils were less potent seeds compared with uncoated fibrils as evident by the right-shift of the ThT curve. The effect was concentration-dependent, and incubation with 5 and 10 μM Bri2 BRICHOS resulted in an almost complete elimination of the seeding capacity and reached a lag phase comparable with the 6 h determined for monomeric IAPP. Addition of 20 μM Bri2 BRICHOS inhibited the seeding capacity and aggregation of IAPP. Each data point represents mean ± SD ($n = 5$).

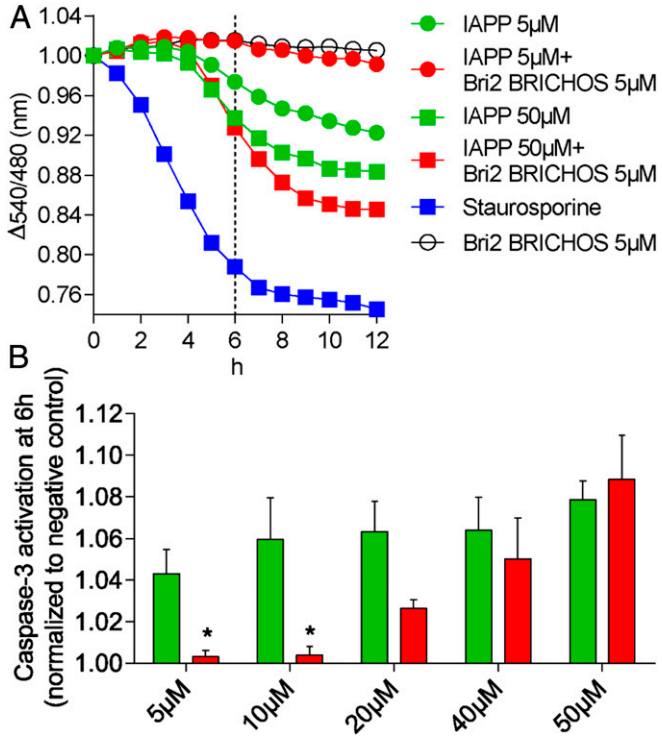

Fig. 8. Bri2 BRICHOS attenuates IAPP-induced cellular caspase-3 activation. Bri2 BRICHOS effect on IAPP-induced apoptosis was monitored using CHO cells expressing a FRET-based reporter for caspase-3 activation. Activated caspase-3 initiates apoptosis and cleaves the reporter proteins, resulting in decreased FRET measured as reduced 540/480 nm ratio at 440 nm excitation. (*A*) FRET measurements were performed in KRGH buffer, pH 7.4, at 37 °C with IAPP alone (5 and 50 μM, green symbols) or in the presence of a constant concentration of Bri2 BRICHOS (5 μM, red symbols). Staurosporine served as positive control and only Bri2 BRICHOS as negative control. (*B*) Processed data on time point 6 h from 5 and 50 μM (*A*) and from concentrations10, 20, and 40 μM IAPP. For clarity data were inverted from decreased FRET into increased caspase-3 activation and normalized to negative control. Bri2 BRICHOS (5 μM) effectively attenuated IAPP-induced caspase-3 activation at lower IAPP concentrations (5 and 10 μM) but not at higher IAPP concentrations (20, 40, and 50 μM). Unpaired Student's *t* test, $*P < 0.05$. Mean ± SEM ($n = 4$ to 7 trials, each performed on different days and based on three repeats). Green bars are 5, 10, 20, 40, and 50 μM IAPP and red bars are 5, 10, 20, 40, and 50 μM IAPP with 5 μM Bri2 BRICHOS.

(Bri2-siRNA) to knock down Bri2 and achieved successful degradation of Bri2 mRNA, as demonstrated by reduced levels of Bri2 mRNA with qRT-PCR (Fig. 9*A*) and immunostaining with anti-Bri2 78–224 of Bri2-siRNA–treated EndoC-βH1 cells (Fig. 9 *B* and *C*). EndoC-βH1 cells were treated with Bri2-siRNA or nontargeting siRNA, and, after 66 h, transfection medium was replaced with medium containing normal glucose (5.5 mM), high glucose (28 mM), high sodium palmitate (SP) (1.5 mM SP), or a combination of high glucose and high SP concentrations, mimicking a gluco- and/or lipotoxic environment. After 48 h culture, cells were fixed and analyzed. EndoC-βH1 cells grow as a monolayer and require adhesion to surfaces for survival, and, as a consequence of death, they lose their adherence properties and detach. Markedly fewer Bri2-siRNA–transfected cells remained attached to the bottom of the wells when exposed to high SP concentration or a combination of high SP and high glucose, compared with nontargeting siRNA-treated cells exposed to the same condition (Fig. 9*D*).

To investigate if the BRICHOS domain was sufficient for counteracting the increased sensitivity to beta-cell stress, we produced adenovirus for overexpression of the Bri2 BRICHOS domain (Ad-Bri2-BRICHOS) in the secretory pathway. EndoC-βH1 cells were transfected with Bri2-siRNA or nontarget siRNA, and, after 18 h incubation, Ad-Bri2 BRICHOS was added and cells were incubated an additional 48 h. Cell culture medium was replaced as above, and, after 48 h of culture, cells were fixed and the area of attached cells was determined (Fig. 9*D*). EndoC-βH1 cells first treated with Bri2-siRNA to reduce endogenous Bri2, followed by viral overexpression of the BRICHOS domain, were no longer susceptible to beta-cell stress, and cells cultured at high SP or high SP and high glucose survived to almost the same degree as control cells treated with nontargeting siRNA or nontargeting siRNA and Ad-Bri2-BRICHOS (Fig. 9*D*). EndoC-βH1 cells exposed to high SP and high glucose increase their IAPP secretion without a concomitant increase in insulin secretion (34). A scenario with high levels of IAPP in the secretory pathway with a concurrent reduction of antiamyloid chaperone Bri2 could be detrimental for the cells and induce cell death. Overexpression of Bri2 BRICHOS domain after silencing of endogenous Bri2 production abrogated almost completely cell toxicity and strengthens the proposition that Bri2 and more precisely its BRICHOS domain can function as a chaperone and modulate IAPP toxicity.

EndoC-βH1 cells transfected with siRNA and cultured in high glucose, high SP, or a combination of high glucose and high SP were incubated with 3 μM pFTAA in PBS. pFTAA is an amyloid-specific polyelectrolyte (LCO) also shown to detect preamyloid aggregates. After labeling with pFTAA, cells were scrutinized for amyloid in a fluorescence microscope (35). Despite extensive analysis, it was not possible to detect amyloid or preamyloid formations in these cells, independent of treatment.

Bri2 BRICHOS Reduces IAPP Toxicity in *Drosophila* Brain Cells. To investigate Bri2 BRICHOS effects on intracellular toxicity of IAPP in vivo, we used *Drosophila melanogaster* as a model organism. The pdf driver (36) was used to direct transgenic expression of IAPP, Bri2 BRICHOS, or the combination thereof to eight lateral ventral neurons (LNvs) present in each eye lobe of the fly brain. The Bri2 BRICHOS domain construct, which lacks the transmembrane ER-targeting segment of full-length Bri2, was directed to the secretory pathway by insertion of an upstream signal peptide. Nuclear leading sequence (nls) GFP was used to facilitate identification of these LNvs (Fig. 10*A*). IAPP expression resulted in a loss of detected LNvs compared with control flies expressing nls GFP only (Fig. 10*B*), which can be interpreted as a result of cell death due to IAPP-induced toxicity. This suggests that toxic IAPP species are formed intracellularly. Coexpression of IAPP together with Bri2 BRICHOS prevented the toxic effects induced by IAPP, and the number of detected LNvs was similar as observed in control flies. Expression of Bri2 BRICHOS alone did not change the number of detected LNvs. These data demonstrate that the toxic effects exerted by IAPP expression in the secretory pathway of a *Drosophila* cell can be alleviated by the concomitant expression of Bri2 BRICHOS.

Concluding Discussion

With this work, we aimed to investigate whether Bri2 associates with and affects IAPP fibril formation, a process linked to the loss of beta cells observed in T2D. IAPP is one of the most amyloidogenic peptides described, and the existence of an endogenous inhibitor was anticipated. Bri2 is expressed in the brain and has previously been linked to enzymatic processing of AβPP in AD (3, 4). In addition, the Bri2 BRICHOS domain has been shown to inhibit the aggregation, fibril formation, and toxicity of Aβ (10, 22–25). Here, we show that Bri2 protein is expressed in human islets of Langerhans and, specifically, in islet beta cells, the same cells that secrete IAPP. Bri2 expression in islets is supported by the identification of binding sites for multiple islet-specific transcription factors in flanking regions of the human *ITM2B* gene (37) and by a recent study reporting high levels of Bri2 mRNA in isolated human islets and the EndoC-βH1 cells (38).

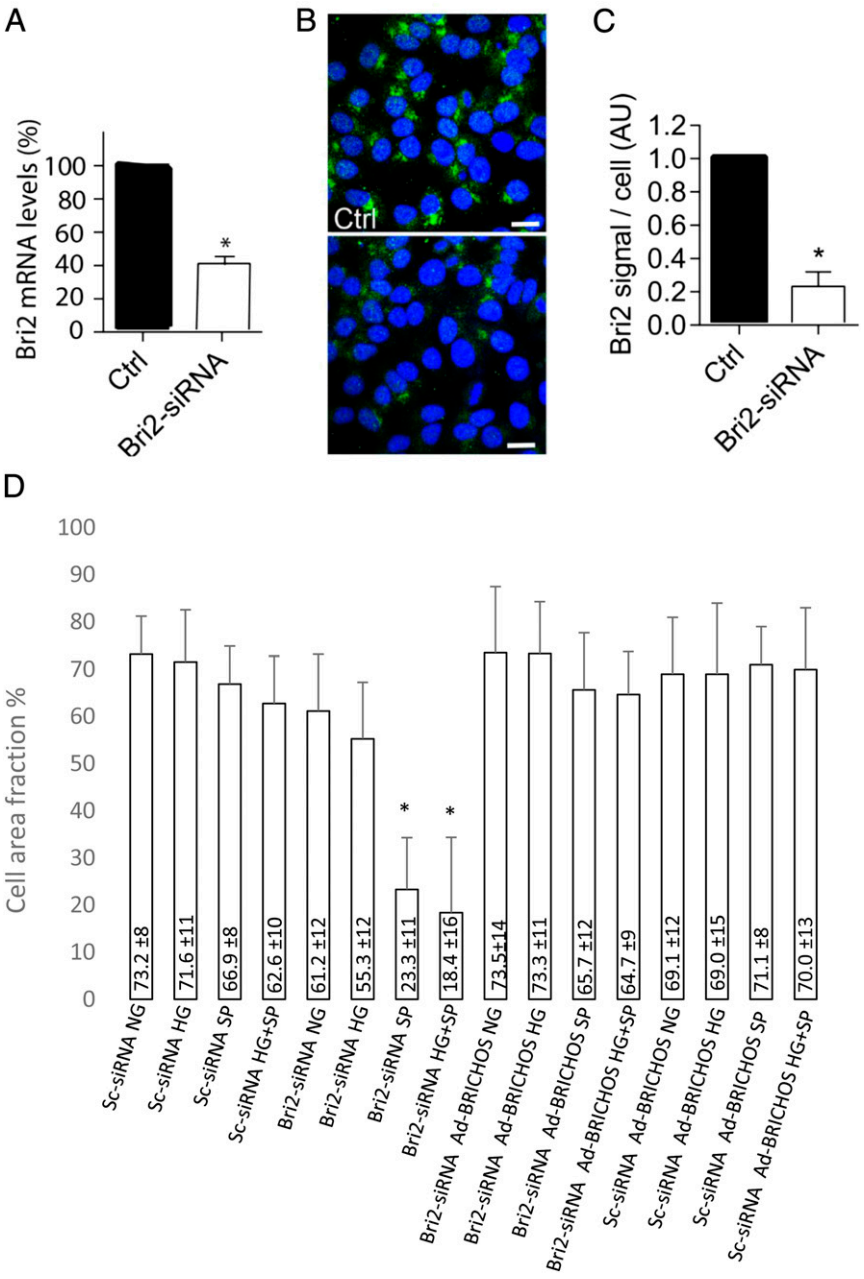

Fig. 9. Expression of Bri2 BRICHOS domain protects EndoC-βH1 from cytotoxicity during stimulatory stress. (*A*) Transfection of EndoC-βH1 with Bri2-siRNA reduced Bri2 mRNA expression levels determined by qRT-PCR and (*B* and *C*) protein levels measured with anti-Bri2 78–224 immunostaining 48 h after transfection. Control cells were transfected with nontargeting siRNA (Ctrl). Data presented relative to Ctrl. Unpaired Student's *t* test, $*P < 0.05$. Mean ± SD ($n = 2$). Images are merged z-stacks acquired with confocal microscopy. (Scale bar: 20 μm.) (*D*) EndoC-βH1 cells transfected with Bri2-siRNA or nontargeting siRNA (Ctrl) with and without subsequent transduction with Ad-Bri2 BRICHOS were exposed to normal glucose (5.5 mM, NG), high glucose (28 mM, HG), high SP (1.5 mM sodium palmitate, SP), or a combination of HG+SP for 48 h. Fewer Bri2-siRNA–transfected cells remained attached to the bottom of the wells compared with Ctrl cells after incubation in SP and HG+SP for 48 h, reflecting increased cell death. In Bri2-siRNA–transfected cells, an overexpression of the Bri2 BRICHOS domain improved cell survival. Two-way ANOVA, Bonferroni's correction, Bri2-siRNA vs. Sc-siRNA, and Bri2-siRNA vs. Bri2-siRNA/Ad-Bri2-BRICHOS, $*P < 0.05$. Mean ± SD ($n = 3$).

The BRICHOS domain of Bri2 prevents the formation of IAPP amyloid fibrils and promotes instead the formation of off-pathway, amorphous aggregates. This is similar to the observed effects of polyphenolic epigallocatechin gallate (EGCG) on IAPP aggregation. Indeed, the presence of EGCG prevented IAPP from forming amyloid fibrils; yet monomers were consumed, and large, nonfibrillar aggregates were formed (39). Monomeric IAPP spontaneously aggregates into amyloid fibrils. However, if this amyloidogenic aggregation pathway is slowed down or prevented, it is possible that IAPP is forced into an alternative aggregation pathway to prevent exposure of its hydrophobic residues. BRICHOS slows down the fibril formation partly by preventing secondary nucleation (30). However, in a milieu favorable for fibrillation (i.e., increased concentration of the amyloid protein), the inhibiting effect is eventually overcome, and fibril formation proceeds, perhaps by recruitment of monomers from the amorphous aggregates. This would explain the higher toxicity observed after prolonged incubation of 50 μM

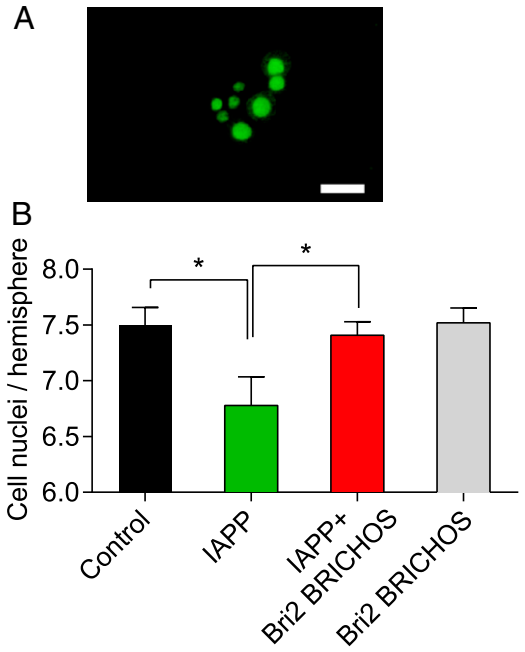

Fig. 10. Bri2 BRICHOS reduces IAPP-induced toxicity on lateral ventral neurons (LNvs) in *D. melanogaster*. (*A*) Expression IAPP and Bri2 BRICHOS was driven to the LNvs of the *Drosophila* brain using nuclear GFP as a reporter protein. (*B*) Transgenic IAPP expression in LNvs resulted in a reduced number of detected LNvs compared with control flies, suggesting cell death due to IAPP toxicity. Coexpressing IAPP with Bri2 BRICHOS had a rescuing effect and prevented the loss of cells, reaching numbers of LNvs comparable with control flies. Expression of Bri2 BRICHOS alone had no effect on LNvs survival. ANOVA, Bonferroni's correction, vs. IAPP, $*P < 0.05$. Mean ± SEM ($n = 27$ to 28 hemispheres). (Scale bar: 20 μm.)

IAPP in the presence of 5 μM Bri2 BRICHOS (Fig. 8), a condition during which Bri2 BRICHOS would extend the fibril formation process and therefore prolong the time period under which toxic oligomers can be formed. If the soluble oligomers are not removed, this could lead to an increase in cell toxicity, despite strong reduction of overall fibril formation. Extrapolated to an in vivo situation, it is conceivable that an elevation of IAPP synthesis without a compensatory increase in Bri2 during beta-cell stress, as observed in the human islets (Fig. S2) and in the Bri2-siRNA–transfected cells (Fig. 9), could be sufficient to tip the balance in favor of toxicity. The finding that the BRICHOS domain of Bri2 could almost fully compensate for the reduction of endogenous Bri2 supports that BRICHOS is a chaperone and that the interaction between IAPP and Bri2 is dependent on the BRICHOS domain. Furthermore, coexpression of IAPP and BRICHOS in LNvs cells in *D. melanogaster* ameliorated IAPP toxicity observed when IAPP was expressed alone (Fig. 10).

In conclusion, we have shown that Bri2 colocalizes with intracellular IAPP in human beta cells and with amyloid deposits. Furthermore, Bri2 BRICHOS inhibits IAPP fibril formation and also reduces toxicity induced by fibrillating IAPP in cell lines and in a *Drosophila* model. These findings make Bri2, in particular its BRICHOS domain, an important component in further studies of IAPP aggregation and toxicity, with the potential to find novel strategies for treating T2D.

Materials and Methods

Human Islets and EndoC-βH1 Cells. Isolated human pancreatic islets from brain-dead donors were obtained from the Nordic Network for Clinical Islet Transplantation (Uppsala University Hospital). Experiments with human islets were approved by the regional ethical committee, Uppsala, Sweden. Human islets were cultured in Connaught Medical Research Laboratories (CMRL) 1066 medium containing 5.5 mM glucose supplemented with 10% (vol/vol) FCS, 100 IU/mL penicillin, 100 μg/mL streptomycin, and 2 mM L-glutamine. Human beta-cell line EndoC-βH1, kindly provided by R. Scharfmann and P. Ravassard (INSERM, Paris) (40), was maintained in DMEM/F12 medium (41) containing 5.5 mM glucose with 0.2% (vol/vol) MycoZap (Lonza), 10 mM nicotinamide, 6.7 ng/mL selenite, 5.5 μg/mL transferrin, 2% (wt/vol) fatty acid-free albumin, 50 μM β-mercaptoethanol, and 2 mM L-glutamine and cultured on ECM/fibronectin (Sigma)-coated surfaces. Islets and cells were cultured at 37 °C in 5% CO_2. For biochemical analysis, islets or cells were washed and lysed by brief sonication in 50 mM Tris·HCl, pH 6.8, 12% glycerol, 4% SDS, 10 mM DTT, and 0.01% Coomassie blue G-250 (SDS sample buffer) and snap frozen in liquid nitrogen.

BRI2 and IAPP mRNA Analysis with Real-Time PCR. Isolated human islets ($n = 3$ donors) were divided into two batches and cultured in normal glucose (5.5 mM) or high glucose (20 mM) for 2 d, after which islets were lysed in Qiazol (Qiagen) and total RNA purified (RNeasy MiniElute cleanup columns; Qiagen). One microgram of RNA was used for first-strand cDNA synthesis with Oligo dT primer (no. K1632; Thermo Scientific). Reactions containing 10 ng of cDNA, 400 nM primer, and FastStart Universal SYBR Green Master (ROX) (Roche Diagnostics) were used for real-time quantitative PCR on a 7900HT Real-Time PCR system (Applied Biosystems). The following primer sequences were used: BRI2, 5′-CTGCAAGGACCC-3′ and 5′-AAACTCTGGGAC-3′; IAPP, 5′-TTTGAGAAGCAATGGGCATC-3′ and 5′-CATGTGGCAGTGTTGCATTT-3′; and GAPDH, 5′-AACTTTGGCATTGTGGAAGG-3′ and 5′-CACATTGGGGGTAGGAACAC-3′. BRI2 primers were from DNA Technology A/S, and IAPP and GAPDH primers were designed with Primer3 and produced at TAG Copenhagen.

Adenoviral-Bri2 Expression System. cDNA encoding a 23-residue signal peptide linked to Bri2 residues 90 to 236 was produced with PCR using forward primer 5′-CGATAAGCTTGCCACCATGGCTGAG-3′ and reverse primer 5′-CAGAGAATTCTCAAGTTTCTCTGCG-3′, and ligated into pacAd5 CMVK-NpA shuttle vector (RAPAd CMV Adenoviral Expression System; Cell Biolabs). Ad-Bri2-BRICHOS shuttle vector (4 μg) and backbone vector (pacAd5 9.2-100; Cell Biolabs) (1 μg) were linearized with PacI (New England Biolabs), mixed with 10 μL of Lipofectamine 2000 Reagent (ThermoFisher Scientific) and added dropwise to HEK293 cells. Amplification and purification of viral stock were performed according to the manufacturer's protocol. Virus titer needed for 90% infection of EndoC-βH1 without visible side effects was determined, and adenovirus Ad-Bri2-BRICHOS was stored at −80 °C.

Bri2-siRNA Transfection and Bri2 BRICHOS Domain Transduction. To reduce endogenous production of Bri2, EndoC-βH1 cells (25,000 cells per well in a 96-well plate with clear bottom) were transfected with 50 nM Bri2-siRNA (5′-CAGAAACCUACUGGAGUUA-3′; Sigma) using 0.25 μL of DharmaFECT per well (Dharmacon) according to the manufacturer's instructions. Control cells were transfected with 50 nM nontargeting siRNA (Dharmacon). EndoC-βH1 cells transfected with Bri2-siRNA or nontargeting siRNA were cultured for 66 h before replacement of culture medium.

To determine if the observed toxicity caused by Bri2 knock down was effected by the BRICHOS domain, EndoC-βH1 cells were transfected with Bri2-siRNA, and, after 18 h, adenovirus Ad-Bri2-BRICHOS was added and cells were cultured for 48 h (in total, 66 h) before replacement of culture medium. Control EndoC-βH1 cells were transfected with nontargeting siRNA, and, after 18 h, adenovirus Ad-Bri2-BRICHOS was added and cells were cultured for 48 h (in total, 66 h) before replacement of culture medium. Ad-Bri2-BRICHOS was diluted in complete medium, and a volume of 50 μL was added to each well. In wells with EndoC-βH1 cells transfected only with Bri2-siRNA or nontarget siRNA, 50 μL complete medium were added. After 66 h, transfection media were removed and cells exposed to Bri2-siRNA, nontarget siRNA, Bri2-siRNA+Ad-Bri2-BRICHOS, and nontarget siRNA+Ad-Bri2-BRICHOS were cultured in complete DMEM/F12 medium with 2% albumin 5.5 mM glucose or stimulatory medium with 28 mM glucose, 1.5 mM SP (sodium palmitate; Sigma) or 28 mM glucose + 1.5 mM SP. After 48 h incubation, medium was replaced by 10% neutral buffered formalin, and images (>30 per incubation) were captured in an inverted microscope (Nikon Eclipse, TE2000-4) supplied with a digital camera (Nikon DXM 1200C). Cell area was determined with ImageJ software.

Recombinant $Bri2_{90–236}$ and $Bri2_{113–231}$. Recombinant protein corresponding to human Bri2 90–236 was expressed as previously described (10). A fragment corresponding to human Bri2 (NP_068839) positions 113 to 231 was expressed as a soluble fusion protein with His_6 and thioredoxin in *Escherichia coli* as previously described (23). Briefly, protein expression was induced with isopropyl-β-D-thiogalactopyranoside (IPTG) for 4 h at 25 °C. Bacteria were lysed and centrifuged at 6,000 × *g* for 20 min. The pellet was suspended in 2 M urea in

CELL BIOLOGY

20 mM sodium phosphate buffer, pH 7.5, sonicated, and centrifuged at 24,000 × *g* for 30 min at 4 °C, and the supernatant was loaded on a 2.5-mL nickel-agarose column (Qiagen). The column was washed in decreasing concentrations of urea (2 M to 1 M), followed by 20 mM imidazole, and, finally, proteins were eluted with 200 mM imidazole. All steps were performed in 20 mM sodium phosphate buffer, pH 7.5. Proteins were dialyzed against 20 mM sodium phosphate buffer, pH 7.5, cleaved by thrombin for 16 h at 4 °C (enzyme/substrate weight ratio of 0.002) to remove thioredoxin and His_6 tag, and reapplied to an Ni^{2+} column to remove the released tag. Concentration was determined from A_{280} using a molar extinction coefficient, $\varepsilon = 9{,}065 \times M^{-1} \times cm^{-1}$.

Slot Blot and Western Blot Analysis. For slot blot analysis, $IAPP_{1–37}$ (Keck Biotechnologies), $A\beta_{1–42}$ (Bachem), $Bri2_{90–236}$, and $Bri2_{113–231}$ were diluted in 50 mM sodium carbonate buffer, pH 9.6, and applied (55 pmol) to a nitrocellulose membrane. For Western blot analysis, islet and cell extracts and recombinant Bri2 proteins were separated by 6 to 12.5% Tricine-SDS/PAGE and transferred onto a nitrocellulose membrane. Membranes were blocked and incubated with the following primary antibodies overnight at 4 °C: goat antiserum against $Bri2_{113–231}$ (anti-Bri2 113–231) (26) 1:2,000; rabbit antibody against $Bri2_{78–224}$ (anti-Bri2 78–224) (HPA029292; Sigma) 1:500; rabbit antiserum A133 against $IAPP_{20–29}$ (42) 1:1,000; and mouse monoclonal 4G8 (Signet) against $A\beta_{17–24}$ 1:1,000. Reactivity was visualized with HRP-conjugated secondary antibodies and chemiluminescence detection.

Quantitative Western Blot. For determination of BRI2 protein levels, anti-BRI2 78–224 reactivity on blots was quantified using ImageJ software and normalized against beta-actin reactivity (Sc1616, 1:1,000; Santa Cruz).

Immunofluorescence and Congo Red Staining. Formalin-fixed paraffin-embedded human pancreas sections were heat-treated in 10 mM sodium citrate, pH 6. EndoC-βH1 cells fixed in 4% paraformaldehyde (PFA) were permeabilized in 0.1% saponin. Incubation with primary antibodies was carried out overnight at 4 °C; anti-Bri2 78–224, anti-Bri2 113–231, anti-insulin (Dako), anti-TGN38 (Santa Cruz), or anti-GM130 (Santa Cruz) were all diluted 1:100, except anti-insulin, which was diluted 1:250. Primary antibodies were detected with secondary antibodies conjugated with Alexa Fluor 488 or Alexa Fluor 546 diluted 1:500 for 1 h. Alkaline Congo red staining of sections was performed according to Puchtler and Sweat (43).

Proximity Ligation Assay. Formalin-fixed and paraffin-embedded sections from pancreas and brain were heated in 10 mM sodium citrate, pH 6 (pancreas) or incubated for 4 min in formic acid (brain). Fixed (4% paraformaldehyde) EndoC-βH1 cells were permeabilized in 0.1% saponin. Incubations with primary antibody combinations, at 1:500 or 1:1,000 dilutions, were carried out overnight at 4 °C. Duolink in situ PLA (Sigma) was performed according to the manufacturer's instructions, with PLA probes diluted 1:5 and amplified oligonucleotide strands visualized with fluorophores excited by a 543-nm laser.

Microscopic Analysis. Immunofluorescence, PLA, and Congo red-stained sections were visualized with a Nikon Eclipse E800 confocal microscope (Nikon), equipped with argon 488 nm, HeNe 543 nm, and LED 405 lasers. Cell area fractions were obtained from bright field images. All image analyses were performed with ImageJ software.

Thioflavin T Assay. ThT assay was performed in 120 mM NaCl, 4.7 mM KCl, 2.5 mM $CaCl_2$, 1.2 mM $MgSO_4$, 0.5 mM KH_2PO_4, pH 7.4, supplemented with 20 mM Hepes and 2 mM glucose (KRGH buffer) with 3 μM ThT in Sigmacote (Sigma)-treated 96-well plates (optical bottom, black sides, polymerbase; NUNC).

A stock solution of IAPP (5 mM, in DMSO; Keck Biotechnologies) was diluted to desired concentrations immediately before the assay, and ThT fluorescence was monitored at 480 nm with 440-nm excitation (44) at 37 °C on a FLUOstar Omega microplate reader (BMG Labtech).

Size-Exclusion Chromatography. IAPP 50 μM or IAPP 50 μM with $Bri2_{113–231}$ 5 μM incubated for 4 h at 37 °C or freshly diluted IAPP or $Bri2_{113–231}$ at the same concentrations were separated on a Superose 12 10/300 GL column (GE Healthcare) in KRGH buffer, pH 7.4, with a flow rate of 0.5 mL/min for 1 h. Collected fractions were applied to a dot blot, and immunoblotting was performed with IAPP antibody A133 or anti-Bri2 113–231 as described above.

Electron Microscopy. Aliquots of aggregated samples (without ThT) were diluted 1:30 in double distilled water, adhered on formvar-coated grids, and subjected to negative stain with 2% uranyl acetate in 50% ethanol or to immunolabeling. For immunoelectron microscopy, grids with adhered samples were blocked in 3% BSA for 30 min and incubated with primary antibodies against Bri2 (anti-Bri2 113–231) or IAPP (SM1341; Acris). Grids were washed in TBS, reblocked in 3% BSA, and incubated with secondary antibodies conjugated with 10-nm gold particles. All antibodies were diluted 1:200 in 1% BSA in TBS and incubated for 2 h at room temperature. After washing, grids were rinsed in double distilled water and negatively stained with 2% uranyl acetate in 50% ethanol. Samples were analyzed at 75 kV in a Hitachi 7100 TEM, and images were obtained with a Gatan 832 Orius SC1000.

Caspase-3 Activation Assay. The FRET-based caspase-3 activation assay using CHO-DEVD cells was performed as described (28). The assay was initiated by diluting IAPP from a stock solution (5 mM, in DMSO; Keck Biotechnologies) with KRGH buffer, pH 7.4, to the specified final concentrations, adding sonicated preformed fibrils (seed) and immediately applying the solution to the plated CHO-DEVD cells and starting FRET measurements. When the effect of Bri2 BRICHOS was tested, recombinant Bri2113–231 (5 μM) was added simultaneously with IAPP to the solutions. IAPP fibril seed corresponding to 125 nM monomeric IAPP was added to ensure consistency of fibrillation between experiments. Staurosporine (1 μM) was applied as positive control and $Bri2_{113–231}$ (5 μM) with seed as negative control. FRET was monitored at 440-nm excitation, with emission measured at 480 nm and 540 nm in a FLUOstar Omega plate reader at 37 °C.

Generation of *D. melanogaster* Strains. The human cDNA sequence of a Bri2 construct containing the BRICHOS domain ($Bri2_{90–236}$, NP_000533), downstream of a sequence coding for the human surfactant protein B signal peptide ($SPB_{1–23}$, NP_000533) (24), was cloned into the pUASTattB, and site-specific insertion on the chromosome 3 86Fb locus was achieved by using the φC31 system (BestGene Inc). *D. melanogaster*-expressing human IAPP behind the human signal peptide was generated earlier (45). W^{1118} was used as background to generate fly strains in a standardized way (46). Fly lines were crossed to achieve the desired transgenes. The Pdf-Gal4 driver was used to direct the transgene expression to the ventrolateral neuron (LNv) cells present in the brain. Each brain hemisphere contains eight LNvs, and a concomitant expression of GFP allows for detection of LNvs in dissected brains, with confocal microscopy. Flies were reared at 24 °C and 40% humidity.

***Drosophila* Pdf Nls Cell Nuclei Count.** Whole brains of 25- to 26-d-old female *Drosophila* were dissected, fixed in 10% formalin, and mounted on glass slides. Images were captured immediately after mounting with a Nikon Eclipse E800 C-1 confocal microscope (Nikon) using a 60× magnification objective and an argon 488-nm laser. Cell nuclei were counted using ImageJ software.

ACKNOWLEDGMENTS. We thank Per Westermark (Uppsala University) for human amyloid tissue; Raphael Scharfmann and Philippe Ravassard (Paris Inserm) for EndoC-βH1 cells; and the Nordic Network for Clinical Islet Transplantation for human islets. This work was supported by grants from the Swedish Research Council (to J.J., J.P., and G.T.W.), the Swedish Diabetes Association (to G.T.W.), the Novo-Nordisk Foundation (to G.T.W.), the Family Ernfors Fund (to G.T.W.), the Swedish Alzheimer's Foundation (to J.P. and G.T.W.), and the Center for Innovative Medicine at Karolinska Institutet (CIMED) (to J.J.).

1. Eisenberg D, Jucker M (2012) The amyloid state of proteins in human diseases. *Cell* 148:1188–1203.
2. Sipe JD, et al. (2016) Amyloid fibril proteins and amyloidosis: Chemical identification and clinical classification International Society of Amyloidosis 2016 Nomenclature Guidelines. *Amyloid* 23:209–213.
3. Matsuda S, Giliberto L, Matsuda Y, McGowan EM, D'Adamio L (2008) BRI2 inhibits amyloid beta-peptide precursor protein processing by interfering with the docking of secretases to the substrate. *J Neurosci* 28:8668–8676.
4. Matsuda S, et al. (2005) The familial dementia BRI2 gene binds the Alzheimer gene amyloid-beta precursor protein and inhibits amyloid-beta production. *J Biol Chem* 280:28912–28916.
5. Kim SH, et al. (1999) Furin mediates enhanced production of fibrillogenic ABri peptides in familial British dementia. *Nat Neurosci* 2:984–988.
6. Vidal R, et al. (1999) A stop-codon mutation in the BRI gene associated with familial British dementia. *Nature* 399:776–781.
7. Vidal R, et al. (2000) A decamer duplication in the 3′ region of the BRI gene originates an amyloid peptide that is associated with dementia in a Danish kindred. *Proc Natl Acad Sci USA* 97:4920–4925.
8. Sánchez-Pulido L, Devos D, Valencia A (2002) BRICHOS: A conserved domain in proteins associated with dementia, respiratory distress and cancer. *Trends Biochem Sci* 27:329–332.
9. Martin L, et al. (2008) Regulated intramembrane proteolysis of Bri2 (Itm2b) by ADAM10 and SPPL2a/SPPL2b. *J Biol Chem* 283:1644–1652.

10. Peng S, Fitzen M, Jörnvall H, Johansson J (2010) The extracellular domain of Bri2 (ITM2B) binds the ABri peptide (1-23) and amyloid beta-peptide (Abeta1-40): Implications for Bri2 effects on processing of amyloid precursor protein and Abeta aggregation. *Biochem Biophys Res Commun* 393:356–361.
11. Hedlund J, Johansson J, Persson B (2009) BRICHOS–A superfamily of multidomain proteins with diverse functions. *BMC Res Notes* 2:180.
12. Knight SD, Presto J, Linse S, Johansson J (2013) The BRICHOS domain, amyloid fibril formation, and their relationship. *Biochemistry* 52:7523–7531.
13. Kim J, et al. (2013) Normal cognition in transgenic BRI2-Aβ mice. *Mol Neurodegener* 8: 15.
14. Willander H, Hermansson E, Johansson J, Presto J (2011) BRICHOS domain associated with lung fibrosis, dementia and cancer–A chaperone that prevents amyloid fibril formation? *FEBS J* 278:3893–3904.
15. Westermark P, et al. (1987) Amyloid fibrils in human insulinoma and islets of Langerhans of the diabetic cat are derived from a neuropeptide-like protein also present in normal islet cells. *Proc Natl Acad Sci USA* 84:3881–3885.
16. Westermark P, Andersson A, Westermark GT (2011) Islet amyloid polypeptide, islet amyloid, and diabetes mellitus. *Physiol Rev* 91:795–826.
17. Westermark GT, Krogvold L, Dahl-Jorgensen K, Ludvigsson J (2017) Islet amyloid in recent-onset type 1 diabetes-the DiViD study. *Ups J Med Sci* 122:201–203.
18. Gasa R, Gomis R, Casamitjana R, Novials A (2001) High glucose concentration favors the selective secretion of islet amyloid polypeptide through a constitutive secretory pathway in human pancreatic islets. *Pancreas* 22:307–310.
19. Westermark GT, Gebre-Medhin S, Steiner DF, Westermark P (2000) Islet amyloid development in a mouse strain lacking endogenous islet amyloid polypeptide (IAPP) but expressing human IAPP. *Mol Med* 6:998–1007.
20. Gurlo T, et al. (2010) Evidence for proteotoxicity in beta cells in type 2 diabetes: Toxic islet amyloid polypeptide oligomers form intracellularly in the secretory pathway. *Am J Pathol* 176:861–869.
21. Tsachaki M, et al. (2011) Glycosylation of BRI2 on asparagine 170 is involved in its trafficking to the cell surface but not in its processing by furin or ADAM10. *Glycobiology* 21:1382–1388.
22. Willander H, et al. (2012) BRICHOS domains efficiently delay fibrillation of amyloid β-peptide. *J Biol Chem* 287:31608–31617.
23. Del Campo M, et al. (2015) BRI2 ectodomain affects Aβ42 fibrillation and tau truncation in human neuroblastoma cells. *Cell Mol Life Sci* 72:1599–1611.
24. Poska H, et al. (2016) Dementia-related Bri2 BRICHOS is a versatile molecular chaperone that efficiently inhibits Aβ42 toxicity in Drosophila. *Biochem J* 473:3683–3704.
25. Arosio P, et al. (2016) Kinetic analysis reveals the diversity of microscopic mechanisms through which molecular chaperones suppress amyloid formation. *Nat Commun* 7: 10948.
26. Del Campo M, et al. (2014) BRI2-BRICHOS is increased in human amyloid plaques in early stages of Alzheimer's disease. *Neurobiol Aging* 35:1596–1604.
27. Knight JD, Miranker AD (2004) Phospholipid catalysis of diabetic amyloid assembly. *J Mol Biol* 341:1175–1187.
28. Oskarsson ME, et al. (2015) Heparan sulfate proteoglycans are important for islet amyloid formation and islet amyloid polypeptide-induced apoptosis. *J Biol Chem* 290: 15121–15132.
29. Cohen SI, et al. (2013) Proliferation of amyloid-β42 aggregates occurs through a secondary nucleation mechanism. *Proc Natl Acad Sci USA* 110:9758–9763.
30. Cohen SIA, et al. (2015) A molecular chaperone breaks the catalytic cycle that generates toxic Aβ oligomers. *Nat Struct Mol Biol* 22:207–213.
31. Paulsson JF, Andersson A, Westermark P, Westermark GT (2006) Intracellular amyloid-like deposits contain unprocessed pro-islet amyloid polypeptide (proIAPP) in beta cells of transgenic mice overexpressing the gene for human IAPP and transplanted human islets. *Diabetologia* 49:1237–1246.
32. Lin CY, et al. (2007) Toxic human islet amyloid polypeptide (h-IAPP) oligomers are intracellular, and vaccination to induce anti-toxic oligomer antibodies does not prevent h-IAPP-induced beta-cell apoptosis in h-IAPP transgenic mice. *Diabetes* 56: 1324–1332.
33. Zhang S, Liu H, Yu H, Cooper GJ (2008) Fas-associated death receptor signaling evoked by human amylin in islet beta-cells. *Diabetes* 57:348–356.
34. Krizhanovskii C, Fred R, Oskarsson M, Westermark G, Welsh N (2017) Addition of exogenous sodium palmitate increases the IAPP/insulin mRNA ratio via GPR40 in human EndoC-βH1 cells. *Ups J Med Sci* 122:149–159.
35. Sjölander D, et al. (2016) Establishing the fluorescent amyloid ligand h-FTAA for studying human tissues with systemic and localized amyloid. *Amyloid* 23:98–108.
36. Rezával C, Werbajh S, Ceriani MF (2007) Neuronal death in Drosophila triggered by GAL4 accumulation. *Eur J Neurosci* 25:683–694.
37. Pasquali L, et al. (2014) Pancreatic islet enhancer clusters enriched in type 2 diabetes risk-associated variants. *Nat Genet* 46:136–143.
38. Fred RG, et al. (2015) Role of the AMP kinase in cytokine-induced human EndoC-βH1 cell death. *Mol Cell Endocrinol* 414:53–63.
39. Suzuki Y, Brender JR, Hartman K, Ramamoorthy A, Marsh EN (2012) Alternative pathways of human islet amyloid polypeptide aggregation distinguished by (19)f nuclear magnetic resonance-detected kinetics of monomer consumption. *Biochemistry* 51:8154–8162.
40. Ravassard P, et al. (2011) A genetically engineered human pancreatic β cell line exhibiting glucose-inducible insulin secretion. *J Clin Invest* 121:3589–3597.
41. Krizhanovskii C, et al. (2017) EndoC-βH1 cells display increased sensitivity to sodium palmitate when cultured in DMEM/F12 medium. *Islets* 9:e1296995.
42. Paulsson JF, Westermark GT (2005) Aberrant processing of human proislet amyloid polypeptide results in increased amyloid formation. *Diabetes* 54:2117–2125.
43. Puchtler H, Sweat F (1965) Congo red as a stain for fluorescence microscopy of amyloid. *J Histochem Cytochem* 13:693–694.
44. Gade Malmos K, et al. (2017) ThT 101: A primer on the use of thioflavin T to investigate amyloid formation. *Amyloid* 24:1–16.
45. Schultz SW, Nilsson KP, Westermark GT (2011) Drosophila melanogaster as a model system for studies of islet amyloid polypeptide aggregation. *PLoS One* 6:e20221.
46. Spradling AC, Rubin GM (1982) Transposition of cloned P elements into Drosophila germ line chromosomes. *Science* 218:341–347.